

Journal of Biomedical Optics

SPIEDigitalLibrary.org/jbo

Tiny endoscopic optical coherence tomography probe driven by a miniaturized hollow ultrasonic motor

Tianyuan Chen
Ning Zhang
Tiancheng Huo
Chengming Wang
Jing-gao Zheng
Tieying Zhou
Ping Xue

Tiny endoscopic optical coherence tomography probe driven by a miniaturized hollow ultrasonic motor

Tianyuan Chen,^a Ning Zhang,^{a,b} Tiancheng Huo,^a Chengming Wang,^a Jing-gao Zheng,^a Tieying Zhou,^a and Ping Xue^a

^aTsinghua University, Department of Physics and State Key Laboratory of Low-Dimensional Quantum Physics, Beijing 100084, China

^bMassachusetts Institute of Technology, Department of Electrical Engineering and Computer Science and Research Laboratory of Electronics, Cambridge, Massachusetts 02139

Abstract. We present an endoscopic probe for optical coherence tomography (OCT) equipped with a miniaturized hollow ultrasonic motor that rotates the objective lens and provides an internal channel for the fiber to pass through, enabling 360 deg unobstructed circumferential scanning. This probe has an outer diameter of 1.5 mm, which is ultra-small for motorized probes with an unobstructed view in distal scanning endoscopic OCT. Instead of a mirror or prism, a customized aspheric right-angle lens is utilized, leading to an enlargement of the numerical aperture and thus high transverse resolution. Spectral-domain OCT imaging of bio-tissue and a phantom are demonstrated with resolution of $7.5 \mu\text{m}$ (axial) \times $6.6 \mu\text{m}$ (lateral) and sensitivity of 96 dB. © The Authors. Published by SPIE under a Creative Commons Attribution 3.0 Unported License. Distribution or reproduction of this work in whole or in part requires full attribution of the original publication, including its DOI. [DOI: 10.1117/1.JBO.18.8.086011]

Keywords: optical coherence tomography; endoscopic probe; hollow ultrasonic motor.

Paper 130167PR received Mar. 24, 2013; revised manuscript received Jul. 8, 2013; accepted for publication Jul. 16, 2013; published online Aug. 16, 2013.

1 Introduction

Optical coherence tomography (OCT) is an emerging modality for obtaining cross-sectional images.¹ As a noninvasive cross-sectional imaging technique with micrometer resolution, OCT has become very promising in the field of biomedical applications. Due to limitation of the light penetration, small and high-resolution probes for endoscopic OCT have been regarded as powerful tools in examining internal organs.² There have been various designs of endoscopic OCT probes over the past decade,^{3–6} which can be divided into two groups based on the scanning modes: forward scanning and circumferential scanning. Among them, circumferential probes are utilized extensively for imaging within hollow tissues, such as arteries, esophagus, and colon.⁷ For the circumferential scanning probes, the scanning can be implemented in two ways based on their driving modes:⁸ proximal scanning or distal scanning.

One common design of proximal scanning probes is implemented by rotating the whole optical fiber at the distal end and the objective lens are fixed with the fiber.^{9,10} However, the fiber is irregularly twisted in the proximal scanning, causing unstable polarization distortion. The rotation may be nonuniform due to the irregular passageway, such as arterial bifurcation. Therefore proximal scanning suffers from the inevitable distortion and artifacts in the recorded OCT images.

In recent years, distal scanning is of high interest, which is mainly implemented by attaching the deflection prism to a micro-motor at the distal end. In this case, the whole fiber remains stationary, so the twisting and nonuniformity problems are avoided.¹¹ Nevertheless, this design has two challenges. One is the wire-shadow effect resulting from the light blocked by power wires, making a portion of the image invisible. The

other is the challenge of miniaturizing the probe due to the complex fabrication of a micro-motor. In fact, many novel technologies have emerged to solve those problems, such as micro-electromechanical systems (MEMS)^{4,6,12} and squiggle motor.¹³ Due to the small size of the endoscopic probes, the numerical aperture of the objective lens is limited and thus the lateral resolution is lower than $10 \mu\text{m}$ ^{4,6,8–13} in distal scanning probes. Meanwhile, to our knowledge, the current smallest distal scanning probe is 1.1 mm in diameter but suffers from wire-shadows,¹⁴ and the outer diameter of the reported smallest shadow-free distal scanning probe is 2.4 mm.¹³

In this article, we propose a new stationary-fiber ultra-small probe, which is equipped with a novel miniaturized hollow ultrasonic motor and a custom-designed objective lens to achieve high lateral resolution. The novel hollow ultrasonic motor enables the fiber to pass through its inside and permits having the fiber, the objective lens and the motor on the same side, enabling 360 deg imaging without any shadow resulted from light blocking by the power wires as in the traditional motor-driven endoscopic OCT. Instead of the traditional prism, an aspheric right-angle lens is utilized to be the last optics surface that optimized the size of the light spot. This probe achieves an outer diameter of 1.5 mm, which is ultra-small for shadow-free rotary probe in distal scanning endoscopic OCT.

2 Device Design

The design scheme of our probe is demonstrated in Fig. 1, which can be divided into the ultrasonic motor and the rotary lens.

The ultrasonic motor is an actuator utilizing piezoelectric material. In this case, our home-made hollow motor is 7 mm in length (with the rotor), 0.7 mm in side length and 36 mg in weight. Four pieces of piezoelectric plates are bonded to the sides of a brass square column ($0.6 \times 0.6 \times 4 \text{ mm}^3$). At its center, an internal channel with a diameter of $\sim 250 \mu\text{m}$ allows the fiber to pass through the whole motor and be fixed steadily with a protection needle (31-gauge). A tiny

Address all correspondence to: Ping Xue, Tsinghua University, Department of Physics and State Key Laboratory of Low-Dimensional Quantum Physics, Haidian District, Beijing, 100084 China. Tel: 86-10-62784531-197; Fax: 86-10-62781598; E-mail: xuep@tsinghua.edu.cn

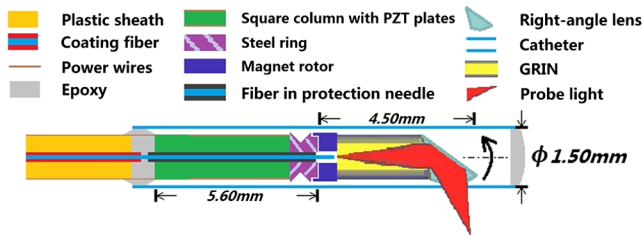


Fig. 1 Schematic of the stationary-fiber rotary scanning optical coherence tomography (OCT) probe driven by a hollow ultrasonic motor.

steel ring (0.8 mm outer diameter, 0.36 mm inner diameter, and 0.8 mm height) is bonded at the upper end of column to assemble the stator, which transfers torque to the magnet rotor (1 mm outer diameter, 0.4 mm inner diameter, and 1.2 mm height). When two sinusoidal signals with $\pi/2$ phase difference between adjacent signals are given to the motor with one end fixed, the piezoelectric plates undergo expansion or contracting sequentially, causing the stator to bend ultrasonic vibration,¹⁵ creating an orbital “hula hoop” motion either clockwise or anti-clockwise. The hollow rotor is then rotated by the friction when there is a pressure supplied by the magnetic force between the steel ring and magnet rotor. The phase shift between two channel waves reverses the direction of the orbit and hence changes the rotation direction of the rotor.

Compared with an electromagnetic motor, an ultrasonic motor possesses the following features: (1) 3 to 10 times larger output power density; (2) smaller responding time (microsecond); (3) no electromagnetic interference; (4) the position of the rotor is self-holding since there exists a large friction force between the rotor and stator. Ultrasonic motors have various, flexible and simple structures that make them the best candidates for micro-motors and MEMS application. Up to now, the ultrasonic motor has been applied in auto-focusing systems of cameras, precision instruments, automobiles, aerospace shuttles and medical instruments.

As shown in Fig. 1, the light emitted from the fiber is first collimated by an 8 deg angled gradient index lens (GRIN) (Towgroup, China), which is combined with the hollow rotor, and then deflected by the right-angled lens for focusing. The custom-designed right-angle lens is equivalent to a prism plus an aspheric lens, which is cut from a commercially available aspheric lens (LightPath) that is made of D-ZLAF52LA glass. The reflecting surface is coated with silver by evaporation to enhance its reflectivity. The tilt angle of the right-angle lens is 53 deg to reduce the back reflection. The rotor, GRIN and right-angle lens are glued by ultraviolet-curing epoxy (Norland Optical Adhesive 61, USA). So the circumferential scanning is realized by the rotation of the rotor.

In the traditional motorized distal scanning probe,¹⁰ there is spacing between the GRIN and deflection prism, leading to a length increase of the rigid part. Our design eliminates this spacing as the GRIN and right-angle lens are glued together, which further shortens the length of the rigid part. Currently, the length of rigid part of our probe is 14 mm, which can be easily shortened to 10 mm by utilizing a shorter catheter. Besides, the fiber, the objective lens and the motor are on the same side in our design, as shown in Fig. 1. The wires are not in the light path and thus do not disturb the imaging, providing 360 deg unobstructed view for endoscopic OCT.

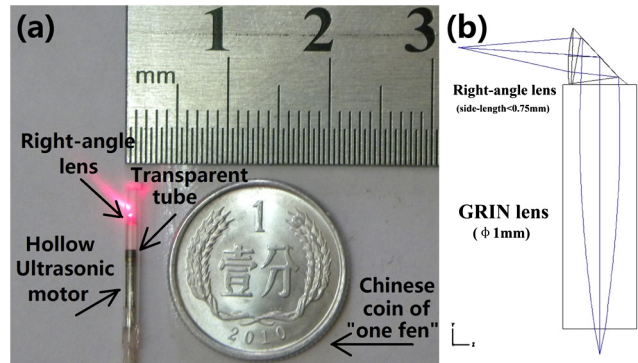


Fig. 2 (a) Photo of the probe with an outer diameter of 1.5 mm. (Video 1, QuickTime, MOV, 10.4 MB) [URL: <http://dx.doi.org/10.1117/1.JBO.18.8.086011.1>] 650 nm laser light emitted from the probe is for demonstration. (b) A ZEMAX layout of the right-angle lens and GRIN lens.

The maximum diameter of the motor and lens is 1 mm. As shown in Fig. 2(a), this prototype probe is installed in a transparent tube (DURAN glass tube, USA) with an outer diameter of 1.5 mm and wall thickness of 0.1 mm. A drawing of the right-angle lens and GRIN lens is demonstrated in Fig. 2(b). A video of the rotation of the probe is available online (Video 1). The speed of rotation is nearly proportional to the driving voltage with a fluctuation of <2% in speed, as shown in Fig. 3(b). The speed, with a torque of $\sim 4 \mu\text{Nm}$, is 2,000 rpm under the driving voltage of 7 Vrms and current of 3 mA. Low scanning speed of ~ 2 fps is also available at 1.6 Vrms.

The lateral cross-section of Huygens point spread function (PSF) of the probe is simulated by optical design software ZEMAX, as shown in Fig. 3(a). The theoretical lateral resolution turns out to be $5.6 \mu\text{m}$ according to the full width at half-maximum (FWHM) of PSF. The corresponding depth of field (DOF) is $\sim 80 \mu\text{m}$, which is designed for obtaining the image of adequate cellular layers. Considering the influence of the package catheter, the X, Y-waist of the beam with the catheter is simulated at different location in the focal region, as shown in Fig. 3(c) and 3(d). Currently the astigmatism caused by the catheter is not compensated. This also leads to an increase of the focal length by ~ 0.1 mm. The working distance is then chosen at ~ 1.3 mm with an X, Y-waist (FWHM) of ~ 6.4 and $\sim 6.6 \mu\text{m}$, which is a compromise among working distance, resolution and DOF. The probe is currently used with a peritoneoscope that has an imaging channel of 1.8 mm in diameter. It also has the potential for vascular imaging if its outer diameter is further optimized.

3 Results

To illustrate the performance of our probe, we integrate the probe with a spectral-domain optical coherence tomography (SD-OCT) system. A broadband semiconductor laser diode (Inphenix Inc., Livermore, CA) is used as light source that has a ~ 45 nm FWHM bandwidth centered at 853 nm, corresponding to an axial resolution of $7.1 \mu\text{m}$ ¹⁶ in air as calculated by $\Delta z = 0.44\lambda^2/\Delta\lambda$. The charge-coupled diode (CCD) (AviiVAM2 CL, Camera Link line scan camera, e2v) contains 2048 pixels with the pixel size of $14 \times 14 \mu\text{m}^2$. The dispersion mismatch of the sample and reference arms is well compensated for numerically.

Experimental measurements are given to demonstrate the detailed performance of the probe. Figure 4(a) shows the

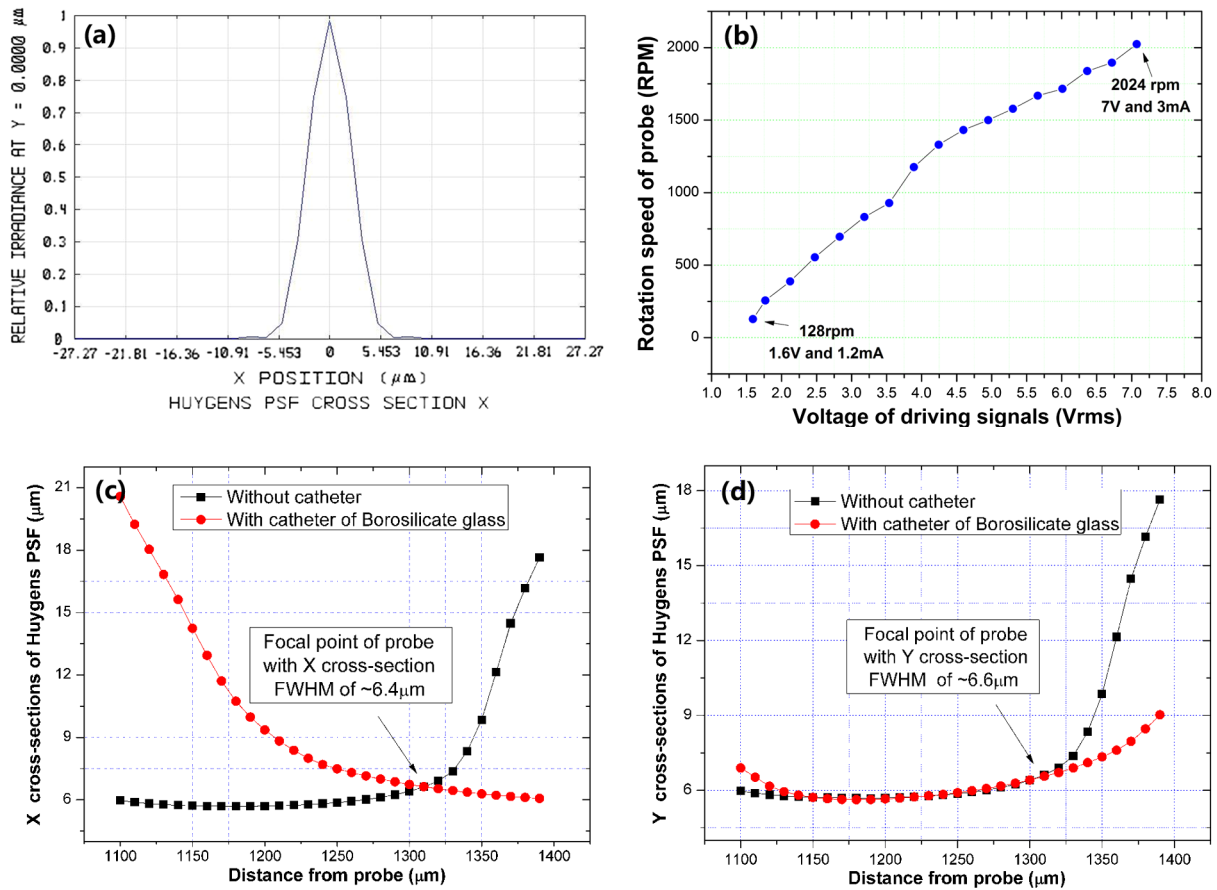


Fig. 3 (a) Lateral cross-section of the Huygens point spread function (PSF) of the spot simulated in ZEMAX. (b) The rotation speed of probe vs. voltage of the driving signals. (c) and (d) Full width at half-maximum of the beam at different location in focal region, which is obtained by x and y cross-sections of the PSFs. Values are calculated in air.

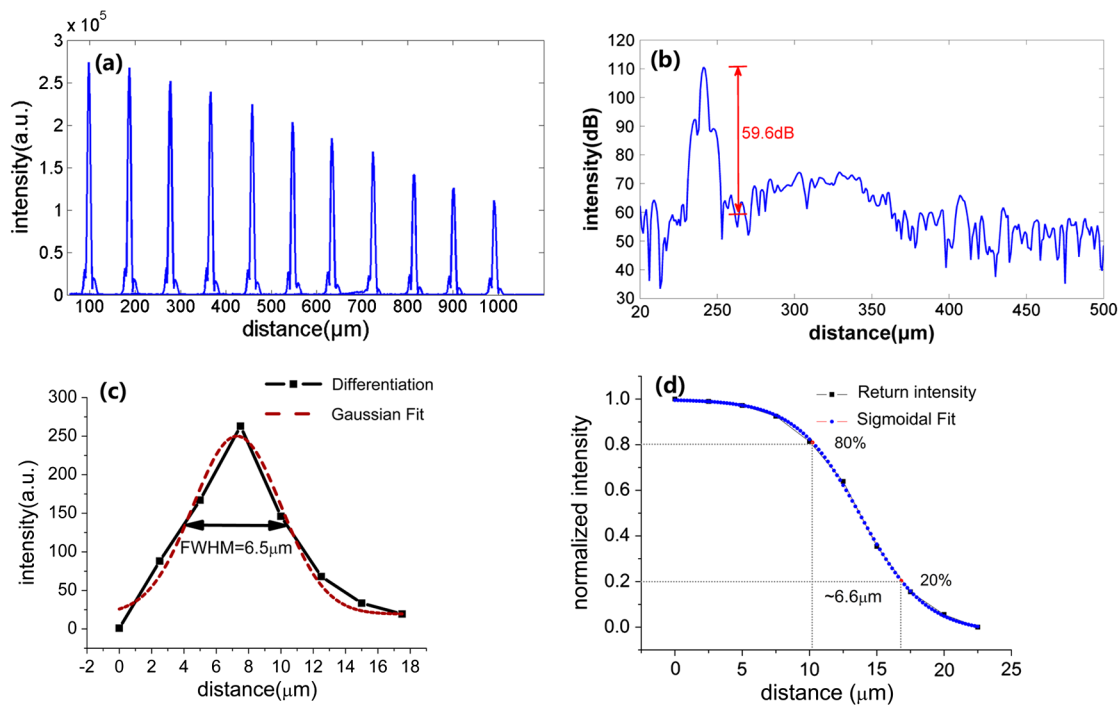


Fig. 4 (a) Axial PSFs obtained by the probe from the working distance. (b) The return signal of 59.6 dB from a sample made of optical-matching gel and BK7 glass. (c) The differentiation of the reflection intensity from a sharp-edge and Gaussian fit. (d) Measurement of the lateral resolution defined as the 20%–80% bandwidth of the curve as $\sim 6.6 \mu\text{m}$.

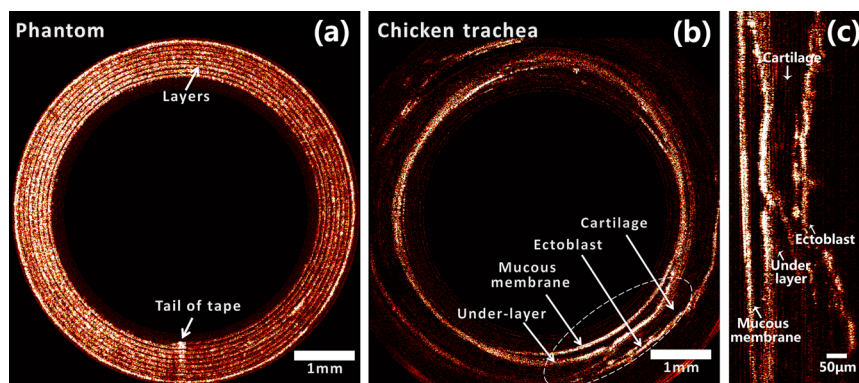


Fig. 5 OCT images obtained with the probe. (a) The phantom of translucent tape. (b) *Ex vivo* chicken trachea tissue. (c) Part of the enlarged image of the dashed region in Fig. 5(b).

axial PSFs at different depths when placing a mirror as the sample. The intensity of the axial PSF decreased 3 dB at the depth of $\sim 800 \mu\text{m}$. Calculated from the FWHM of mirror signal, the axial resolution of the system is $7.5 \mu\text{m}$ in air, which is in agreement with the axial resolution of $7.1 \mu\text{m}$ as calculated from the bandwidth of light source before. To obtain the size of the light spot, we measure the differentiation of relative intensity against lateral position of a sharp-edge of metal film placed at the working distance when the light spot moves over it, as shown in Fig. 4(c) and 4(d). A Gaussian fit of the light intensity gives a FWHM width of $6.5 \mu\text{m}$. The lateral resolution of the probe, as measured with 20% to 80% width of the slope region of the intensity that is measured from the sharp-edge,¹⁷ is $\sim 6.6 \mu\text{m}$, close to the FWHM width of Gaussian fit. The total double-pass return intensity of the probe is 24%, measured by a mirror placed at the working distance. This intensity is strong enough for the CCD to run at an integration time of $50 \mu\text{s}$ for 512 A-scans. A circumferential scan image consists of 5120 A-scans, so the imaging rate is ~ 2 fps with an imaging region of 5120×1024 pixels. To measure the sensitivity of the system, the traditional method of inserting a neutral density filter into the beam path to attenuate the signal is not feasible, as the distance between the focal point and catheter is too small. A special sample is therefore made by optical matching gel (Fibkey, China) and BK7 glass. Fresnel reflection laws give that the reflectivity of their interface is 0.067%, which is also experimentally verified, corresponding to an attenuation of 36 dB. The measured signal-to-noise (S/N) ratio is 59.6 dB, as shown in Fig. 4(b), which means the system sensitivity is ~ 96 dB. The band (centered around $320 \mu\text{m}$) to the right of the signal from the test sample may be caused by the internal coherence from the small spacing of ~ 0.4 mm between the fiber and the GRIN lens.

A phantom was imaged with the probe, as shown in Fig. 5(a), which was made by coiling several layers of translucent tape on a glass tube with an outer diameter of 4 mm and wall thickness of 0.1 mm. The thickness of the tape is $\sim 50 \mu\text{m}$. Currently, post processing is implemented to synchronize the rotation. A trigger from the motor is possible in the future to synchronize the rotation and data-acquisition. The layers of the phantom can be distinguished clearly in the image. The arrow indicates the beginning of the inner first layer. The back reflections from catheter and glass tube are weakened by the mentioned tilt angle. As shown in Fig. 5(b) and 5(c), *ex vivo* imaging of chicken trachea tissue gives the structure of the mucous membrane, the under-layer and the cartilage. The scan depth is about 1 mm. It is clear

that all the images are unobstructed 360 deg views with no shadow effect. Due to limited penetration and strong scattering of ~ 850 nm and relative low depth of focus of the objectives, the quality of image is not good. This may be improved with higher S/N, DOF extending algorithm, proper index matching and dispersion compensation.

4 Conclusions

In conclusion, a novel stationary-fiber rotary endoscopic probe for SD-OCT is proposed. This probe provides an unobstructed 360 deg view for circumferential imaging with a spatial resolution of $7.5 \mu\text{m}$ (axial) \times $6.6 \mu\text{m}$ (lateral) and sensitivity of ~ 96 dB. *Ex vivo* images of chicken trachea and a phantom are shown to demonstrate the performance. The probe has its outer diameter of 1.5 mm, which is ultra-small for shadow-free motorized probe in distal scanning endoscopic OCT.

In this case, the configuration of a hollow motor and right-angle lens has been proved to be a simple, robust and feasible idea for the design of an ultra-small distal scanning probe. The hollow ultrasonic motor not only minimizes the size of entire probe but also reduces the length of rigid part, providing great advantage in the potential applications like vascular endoscopic imaging. There is still room for improvement in design, for this work is in experimental stage. In fact, with a new type of hollow rotor that does not limit the size of aperture at the bottom of GRIN lens, the actual working distance can be reduced, which is more convenient for practical purposes. More biocompatible catheters like the polycarbonate or Pebax tube will be used in our next version. For the convenience in practice, the tip of endoscopy will be sealed by a short transparent catheter with radius designed to match the working distance. This tip will be put in contact with the surface of the lesion, insuring that the tissue is in focus. These results and discussions imply that this design is promising in the future development of endoscopic OCT for clinical applications.

Acknowledgments

This work was supported in part by the National Natural Science Foundation of China under Grant 61227807, by the Ministry of Science and Technology of China under contracts 2006AA02Z472, 001CB510307, and 2009CB929400, by the Ministry of Education of China Grant 20130002110079 for Doctoral Program, and by the Tsinghua Initiative Scientific Research Program Grant 2013THZ02-3. The first two authors contribute equally to this paper.

References

1. D. Huang et al., "Optical coherence tomography," *Science* **254**(5035), 1178–1181 (1991).
2. G. J. Tearney et al., "In vivo endoscopic optical biopsy with optical coherence tomography," *Science* **276**(5321), 2037–2039 (1997).
3. P. R. Herz et al., "Micromotor endoscope catheter for in vivo, ultrahigh-resolution optical coherence tomography," *Opt. Lett.* **29**(19), 2261–2263 (2004).
4. K. H. Kim et al., "Two-axis magnetically-driven MEMS scanning catheter for endoscopic high-speed optical coherence tomography," *Opt. Express* **15**(26), 18130–18140 (2007).
5. K. Aljaseem et al., "Integrated three-dimensional scanner for endoscopic optical coherence tomography," *Proc. SPIE* **7716**, 77162P (2010).
6. X. Mu et al., "Compact MEMS-driven pyramidal polygon reflector for circumferential scanned endoscopic imaging probe," *Opt. Express* **20**(6), 6325–6339 (2012).
7. G. J. Tearney et al., "Three-dimensional coronary artery microscopy by intracoronary optical frequency domain imaging," *J. Am. Coll. Cardiol.* **1**(6), 752–761 (2008).
8. Z. Yaqoob et al., "Methods and application areas of endoscopic optical coherence tomography," *J. Biomed. Opt.* **11**(6), 063001 (2006).
9. G. J. Tearney et al., "Scanning single-mode fiber optic catheter-endoscope for optical coherence tomography," *Opt. Lett.* **21**(7), 543–545 (1996).
10. H. L. Fu et al., "Flexible miniature compound lens design for high-resolution optical coherence tomography balloon imaging catheter," *J. Biomed. Opt.* **13**(6), 060502 (2008).
11. P. H. Tran et al., "In vivo endoscopic optical coherence tomography by use of a rotational microelectromechanical system probe," *Opt. Lett.* **29**(11), 1236–1238 (2004).
12. L. Liu et al., "Miniature endoscopic optical coherence tomography probe employing a two-axis microelectromechanical scanning mirror with through-silicon vias," *J. Biomed. Opt.* **16**(2), 026006 (2011).
13. S. Chang et al., "Stationary-fiber rotary probe with unobstructed 360° view for optical coherence tomography," *Opt. Lett.* **36**(22), 4392–4394 (2011).
14. T. Wang, "Intravascular optical coherence tomography imaging at 3200 frames per second," *Opt. Lett.* **38**(10), 1715–1717 (2013).
15. Z. Tieying, "A cylindrical rod ultrasonic motor with 1 mm diameter and its application in endoscopic OCT," *Chin. Sci. Bull.* **50**(8), 826–830 (2005).
16. N. Zhang et al., "Spectral-domain optical coherence tomography with a Fresnel spectrometer," *Opt. Lett.* **37**(8), 1307–1309 (2012).
17. A. Dubois et al., "High-resolution full-field optical coherence tomography with a Linnik microscope," *Appl. Opt.* **41**(4), 805–812 (2002).